

EPSR: Edge Profile Super resolution

Jiun Lee and Joongkyu Kim

Sungkyunkwan University

(16419) 2066, SEOBU-RO, JANGAN-GU, SUWON-SI, GYEONGGI-DO, KOREA

jiwoon94@g.skku.edu, jkkim@skku.edu

Abstract

Recently numerous deep convolutional neural networks(CNNs) have been explored in single image super-resolution(SISR) and they achieved significant performance. However, most deep CNN-based SR mainly focuses on designing wider or deeper architecture and it is hard to find methods that utilize image properties in SISR. In this paper, by developing an “edge-profile” approach based on end-to-end CNN model to SISR problem, we propose an edge profile super resolution(EPSR). Specifically, we construct a residual edge enhance block(REEB), which consists of residual efficient channel attention block(RECAB), edge profile(EP) module, and context network(CN) module. RECAB extracts adaptively rescale channel-wise features by considering interdependencies among channels efficiently. From the features, EP module generates edge-guided features by extracting edge profile itself, and then CN module enhances details by exploiting contextual information of the features. To utilize various information from low to high frequency components, we design a fractal skip connection(FSC) structure. Since self-similarity of the architecture, FSC structure allows our EPSR to bypass abundant information into each REEB block. Experimental results present that our EPSR achieves competitive performance against state-of-the-art methods.

1. Introduction

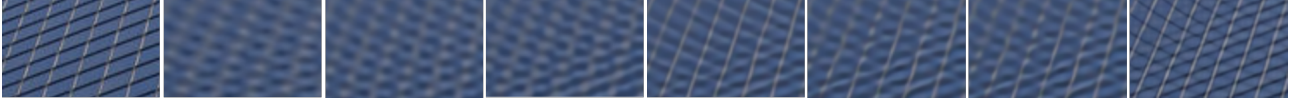
Single image super-resolution(SISR)[14] has been focused on recently. Generally, SISR targets to reconstruct an accurate high resolution(HR) image from its degraded low resolution(LR) image. Image SR is usually applied to diverse computer vision tasks (e.g. security and surveillance imaging[56], object recognition[35], image generation[21], and medical imaging[38]). Since there are plenty of solutions for reconstructing any LR inputs, image SR has an ill-posed inverse[11] problem. To address this issue, numerous SR methods have been proposed, such as interpolation-based[53], model-based[10], image prior methods[47] and

CNN-based methods[8, 55, 7, 22, 46, 28].

The interpolation-based methods are formed as fixed mathematical functions. Although they are simple and efficient, this type of methods is not proper for ill-posed inverse problems. Model-based methods have been proposed to deal with this problem flexibly. Non-local similarity prior[50] and sparsity prior[10] methods apply powerful image prior to produce HR images. Related to image prior methods, image statistical models utilize diverse features, such as gradient distributions[36] of image, to recover HR image. In addition, patch-based models are constructed as mapping function by learning from exemplar patches[5, 13] and edge-based models[12] use edge profile priors to generate sharp HR image. Compared to interpolation-based methods, model-based methods are flexible and effective to generate high quality HR image. However, these methods have time-consuming and process optimization problems. Image prior methods can degrade the performance by image statistics biased from image prior. Since patch-based models are dependent on exemplar patches information, the performance is not uniform. Furthermore, edge-based models are very effective to generate sharp image. However, they have difficulties recovering high frequency information.

Recently, deep convolutional neural networks acquired outstanding results compared with previous methods[16, 5]. Normally, CNN-based models approach SISR problem by utilizing influential feature representation and end-to-end structure. These methods aim to learn mapping function from LR input to its HR output. In this case, LR inputs are generated via downscale functions, such as interpolation operations. CNN-based SISR models[8, 22, 28, 26, 54, 55] achieved notable improvement by using feature information from training dataset. As such, most of CNN-based SR methods just concentrated on constructing deeper or wider networks to utilize high frequency features and important information in LR input. Although these research directions have been very successful, stacking the network deeply to use diverse feature information is not the only way to solve SISR problems.

To search for another breakthrough in SISR research,



(a) HR (b) SRCNN (c) VDSR (d) LapSRN (e) EDSR (f) CARN (g) RCAN (e) Ours

Figure 1. Visual results with Bicubic(BI) degradation($\times 4$) on “img.074” from Urban100. Our method shows better visual quality and recovers more image details compared with other state-of-the-art SR methods.

we revisit image prior in a study by [47]. We take inspiration from past SISR methods based on edge and gradient profile priors [12, 39] to improve the quality of LR image by applying edge and gradient information. These methods are effective in perceptual quality. However, there are limitations in the reconstruction of high frequency features.

To utilize advantages of CNN-based methods, edge and gradient profile prior, we propose an edge profile super resolution (EPSR) for more abundant feature representation including edge feature information generated by CNN-based module. Specifically, we construct a residual edge enhance block (REEB) for learning diverse features involving edge-guided features. Our REEB consists of three modules, which are residual efficient channel attention block (RECAB), edge profile (EP) module, and context network (CN) module. Since RECAB learns feature interdependencies by exploiting mutually independent information, RECAB generates more informative features with high frequency components. EP module generates features that contain edge and gradient profile information by extracting edge and gradient components itself. Then the features contain edge information and high frequency components both. In the end, to learn contextual information in the features from EP module, we construct CN module. It enhances the performance by exploiting multi-scale contextual information. To provide diverse feature information, we design the network by stacking REEBs fractally. Since self-similarity of this structure allows plenty of low frequency components to be bypassed from LR input. We can exploit various information that LR input contains. As in Fig. 1, our method shows competitive visual quality and detail reconstruction compared to the previous deep CNN-based model.

Overall, we can summarize the main contributions of this paper as follows:

- We propose our edge profile super resolution (EPSR) for high-quality image SR using image properties. The network is designed to learn diverse features from original LR image.
- We propose a residual edge enhance block (REEB), which contains 3 modules. First, in residual efficient channel attention (RECAB), we apply efficient channel attention mechanism [44] on SISR to generate adaptive rescale features and to learn inter-dependencies among feature channels efficiently. Edge profile (EP) module then extracts edge profile itself without the help of image-processing tool, such as Canny [4] and Prewitt [34] methods. At the end of the

block, we plug context network (CN) module into EP module. CN module captures contextual information of the features that contain edge information and learn details of the features.

- We propose a fractal skip connection (FSC) structure to build a deep network that bypasses various information from low to high frequency information. Since FSC structure takes self-similarity architecture, it could feed more abundant information not only from LR input but also from each REEB block and keep the training stability of the deep network.

2. Related work

In the computer vision community, various SISR methods have been proposed for several years, such as interpolation-based [53], model-based [10], image prior [47] and CNN-based methods [8, 22, 26, 40, 15, 54, 55, 41]. Since most methods focus on constructing a deep network for utilizing diverse information, it is seldom studied in terms of the image-processing approach nowadays. Due to the limitation of space, we review some works related to our method briefly.

CNN-based model. Recently, CNN-based methods have been mainly studied in single image super resolution. For example, SRCNN proposed by Dong et al. [8] achieve noteworthy performance using three-layer convolutional network. Later, VDSR [22] and DRCN [23] improve accuracy with stacking convolutional networks deeply through residual learning. Tai et al. [40] introduced DRRN, which is a recursive learning model based on parameters sharing and they proposed MemNet [41], which consists of memory block for a deep network. EDSR and MDSR by Lim et al. [28] improve significantly the performance by stacking residual blocks very deeply and widely. From the results, the depth of network is a key point in image SR. Since the achievement of deep networks, RDN by Zhang et al. [55] is designed as a deep network based on the dense block for utilizing all of the hierarchical features from all the convolutional layers. In RCAN [54], they consider not only increasing the depth of network, but also applying feature correlations in spatial and channel dimension.

Attention mechanism. Compared to previous method, attention mechanism SR models achieve significant improvement. In general, previous methods consider uniform importance of all spatial components and channels. However, attention models deal with the features by varying impor-

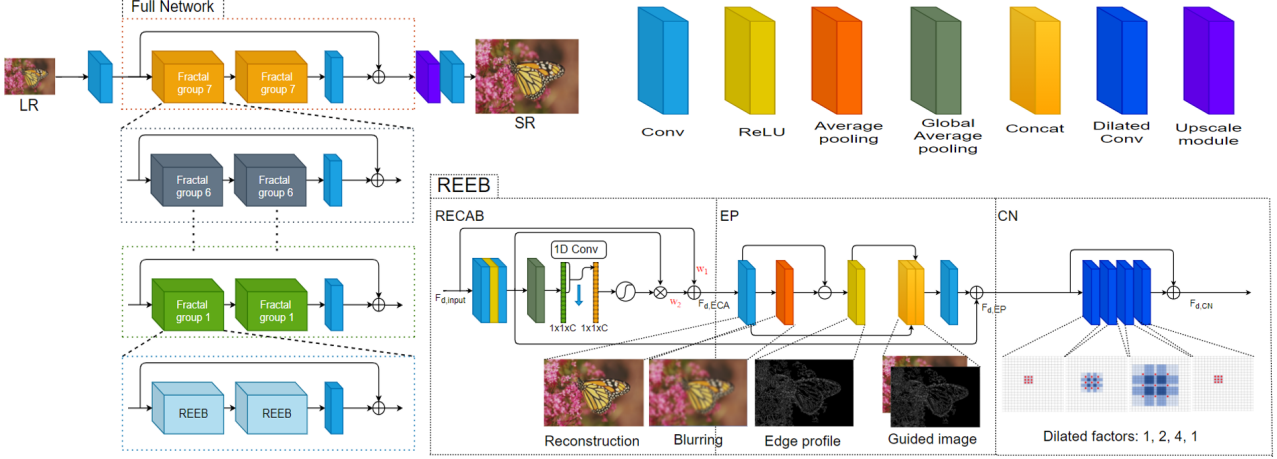


Figure 2. The architecture of the proposed edge profile super resolution (EPSR) and its sub modules.

tance and allow flexibility by helping to selectively attend to a few features at a given layer. Furthermore, Choi et al. [6] introduced Selnets by constructing a selection unit to serve as a check point between convolution layers and allowing only sorted values from the feature maps. DRLN by Anwar et al. [2] consists of pyramid-level attention modeling the features non-linearly to utilize various levels of information. Kim et al. [24] proposed SRRAM utilizing spatial and channel attention for learning the inter-channel and intra-channel dependencies of features.

Edge profile prior. Nowadays, most SR methods only focus on stacking deep network and using diverse information of features. They achieve significant improvement and enlarge the possibility of diverse SR models. Although this trend is very successful in image SR, it is hard to search discussion about applying image properties as edge or gradient components in SISR recently. Since our EPSR is related to the precedent researches, we briefly discuss about edge prior works [12, 39] in image prior SISR.

In visual perception, edge components play a major role. On that basis, edge prior based models apply primarily edge profile priors to reconstruct HR image. The methods, such as the depth and width of an edge [12] or the parameter of a gradient profile [39], reconstruct HR image which contains high quality edge with suitable sharpness and limited artificiality. However, edge profile based models have limitations in recovering high frequency components such as texture. To this end, we propose our EPSR that utilizes edge profile with preventing loss of high frequency information.

3. Proposed Method

3.1. Network Structure

As shown in Fig. 2, our EPSR mainly consists of five parts: shallow feature extraction, fractal skip connection (FSC) structure module, residual edge enhance

block (REEB), which consists of residual efficient channel attention block (RECAB), edge profile (EP) module, and context network (CN) module, upscale module, and reconstruction part. Given I_{LR} and I_{SR} as the input and output of EPSR, as researched in [28, 55], one convolutional layer is applied to extract the shallow feature F_0 from the LR input

$$F_0 = H_{SF}(I_{LR}), \quad (1)$$

where $H_{SF}(\cdot)$ denotes convolution operation and the shallow feature extraction. F_0 is then used for deep feature extraction with FSC module. So we can further get

$$F_{DF} = H_{FSC}(F_0), \quad (2)$$

where $H_{FSC}(\cdot)$ represents a fractal skip connection (FSC) structure module. FSC module consists of residual edge enhance blocks (REEBs), which contain high frequency and edge profile features (see Fig. 2). So our proposed FSC module gains very deep depth and provides thus very large receptive field size. Then the extracted deep feature F_{DF} is upsampled by upscale module as

$$F_{UP} = H_{UP}(F_{DF}), \quad (3)$$

where $H_{UP}(\cdot)$ and F_{UP} stand for upscale module and upsampled feature respectively. For upscaling, there are several modules, such as transposed convolution [9] and ESPCN [37]. Upscaling based on ESPCN obtains a good trade off between computational complexity and performance in the last few layers, and thus is prevail to be used in recent CNN-based SR models [9, 55]. Via one convolution layer, the upsampled feature is then converted into SR image

$$I_{SR} = H_{Re}(F_{UP}) = H_{EPSR}(I_{LR}), \quad (4)$$

where $H_{Re}(\cdot)$, $H_{up}(\cdot)$, and $H_{EPSR}(\cdot)$ denote the reconstruction layer, upscaling layer, and EPSR function, respec-

tively. Then our EPSR is optimized with set-up loss functions. Normally, L_1 [26, 27, 28, 55], L_2 [8, 22, 40, 41], adversarial and perceptual losses[20, 35] have been used in SR method. To establish the effect of EPSR, we choose two loss functions L_1 and $L_{gradient}$ which is gradient loss. As in previous works, we choose L_1 for guaranteeing stable convergence. Let's denote a given training set with N LR images and their HR counterparts as $\{I_{LR}^i, I_{HR}^i\}_{i=1}^N$, and then we can formulate L_1 loss as:

$$L_1 = \frac{1}{N} \sum_{n=1}^{\infty} \|H_{EPSR}(I_{LR}^i) - (I_{HR}^i)\|_1 \quad (5)$$

and then gradient loss can be defined as:

$$L_{gradient} = \frac{1}{N} \sum_{n=1}^{\infty} \|S(H_{EPSR}(I_{LR}^i)) - S((I_{HR}^i))\|_1, \quad (6)$$

where $S(\cdot)$ is gradient function based on Sobel filter[31]. To obtain gradient loss, we find out gradients of ground truth and SR images using Sobel filter, and then apply L_1 loss between gradients of ground truth and SR respectively. At the end, for guiding edge in the training process, we add $L_{gradient}$ to L_1 . The goal of training EPSR is to optimize the total loss function:

$$L_{Total}(\theta) = L_1 + 10^{-1} L_{gradient}, \quad (7)$$

where θ is the parameter set of EPSR. The loss function is optimized by ADAM gradient descent algorithm.

3.2. Fractal Skip Connection

We now show our fractal skip connection(FSC) architecture, which consists of residual edge enhance block(REEB) and fractal patterns of residual network. Previously, to build very deep network, so many proposed methods construct network using combinations of residual and skip connection[28, 55, 54]. However, just simply stacking those kinds of structures would be hard to get better performance. It is an important point to utilize low and high frequency components properly through residual and skip connection.

Inspired by the work in [25], we apply fractal form on skip connections. As we mentioned in section 3.1, fractal skip connection(FSC) structure module is denoted as $H_{FSC}(\cdot)$. The process of this structure can be represented as ignition system.

$$H_{g_k}(F_k) = F_k + f_{conv} \circ H_{g_{k-1}} \circ H_{g_{k-1}}(F_k), \quad (8)$$

where F_k is the input feature of k -th fractal group, H_{g_k} (for $1 \leq k \leq 7$) is the operation of k -th fractal group function, which consists of residual block using two $(k-1)$ -th fractal groups as Fig.2. In the cases of $k = 0$, H_{g_0} is as same as

our REEB. Otherwise, when k is 7, H_{g_k} stands for full architecture of FSC module. Since FSC architecture has self-similarity properties, it can contain lots of complicated skip connections. This complexity of skip connections provides various features that include abundant information from low to high frequency components. Furthermore, this architecture makes it possible to train very deep CNN for SR with high performance and stability.

3.3. Residual Edge enhance block(REEB)

Due to self-similarity of FSC module, the abundant diverse frequency information can be bypassed. To utilize the information from various angles, we design a residual edge enhance block(REEB). Our REEB consists of three modules, residual efficient channel attention block(RECAB), edge profile(EP) module, and context network(CN) module.

Residual efficient channel attention. First, as proposed in EDSR, MDSR[28], by removing batch normalization layers, we extract the feature(see RECAB part of Fig.2). Thus range flexibility of our EPSR can be maintained. So we can formulate feature extraction as

$$F_{d,FE} = H_{FE,d}(F_{d,input}), \quad (9)$$

where the output $F_{d,FE}$ and $H_{FE,d}(\cdot)$ stand for the feature and function from feature extraction of d -th REEB block respectively. $F_{d,input}$ is the input feature of d -th REEB block. However, this feature is equivalent in channel-wise. To give flexibility, attention based-model helps to vary the importance of essential features. Considering feature inter-dependencies and utilizing mutual independence, this type of models has shown noteworthy improvement in SR.

Following the general channel attention process from SENet[17], global average pooling is applied for independence of each channel, and then two convolution layers with non-linearity activated by a sigmoid function generate channel weights of given input feature. Let's denote input feature as X , whose channel dimension is C . Then the weights of channels in channel attention module can be formulated as

$$w = \sigma(W_2 ReLU(W_1(g(X))), \quad (10)$$

where $g(\cdot)$ is channel wise global average pooling (GAP) and σ is a Sigmoid function. ReLU indicates the Rectified Linear Unit, W_1 and W_2 are convolution layers whose sizes are $C \times (\frac{C}{r})$ and $(\frac{C}{r}) \times C$ respectively to avoid computational complexity. The two convolution layers target to capture non-linear cross-channel interaction and it entails dimensionality reduction for controlling model complexity. According to recent research in efficient channel attention(ECA)[44] mechanism, it has been shown that dimensionality reduction brings side effects on channel prediction and captures unnecessary dependencies across all

channels empirically. Furthermore, while channel reduction can decrease model complexity, it messes up the direct correspondence between channel and its weight. To efficiently avoid this problem, ECA captures local cross-channel interaction by using 1D convolution of size k , where kernel size k implies the coverage of local cross-channel interaction and the number of neighbors involved in attention prediction of one channel. To embody this process in equation:

$$w_{eca,d} = \sigma(C1D_k(g(F_{d,FE}))), \quad (11)$$

where $C1D_k$ denotes 1D convolution and $w_{eca,d}$ is the scale statistics of channel. Then $F_{d,FE}$ is rescaled as

$$\hat{F}_{d,FE} = w_{eca,d} \cdot F_{d,FE}, \quad (12)$$

where $\hat{F}_{d,FE}$ stands for rescaled feature.

To utilize informative features from ECA, we apply residual block on the network. Inspired by weighted feature fusion in [42], we transform residual block to use it. In EDSR[28] and RCAN[54], they adopts the residual scaling with factor 0.1 for making the training procedure numerically stable. However, this way can not be the best solution in residual block. So we propose weighted summation on residual block

$$F_{d,RECAB} = \frac{w_1}{\epsilon + \sum_{i=1}^2 w_i} F_{d,input} + \frac{w_2}{\epsilon + \sum_{i=1}^2 w_i} \hat{F}_{d,FE}, \quad (13)$$

where w_i is a learnable weight which is a scalar per feature. As applying a ReLU each w_i , we ensure $w_i \geq 0$, and fix ϵ value as 0.00001 to avoid numerical instability. Similar to interpolation, the values of each weight is ranged from 0 to 1. Since these two weight values are learnable parameters, they find more proper values for producing well-balanced features in every training process.

Edge profile module. To design an end-to-end network and acquire sharp SR image, we focus on how to extract edge information without the help of additional module. So we target to generate edge profile using CNN-based module in our model.

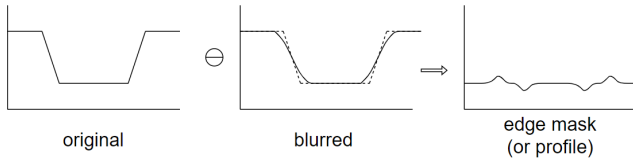


Figure 3. Extracting edge profile process

To understand the properties of edge, we revisit traditional image-processing research. Intuitively, edge area has rapid variance of pixel as Fig.3. This means that there are large pixel gradient values in edge area. Next, the onset and end of discontinuities (e.g. step and ramp discontinuities)

in image are also described as edge areas. To extract edge profile of image, we consider utilizing discontinuous properties of edge. As described in Fig.3, to get edge mask(or profile), we subtract the blurred image from the original. So this process can be formulated as:

$$g(x, y) = f(x, y) - \bar{f}(x, y), \quad (14)$$

where $g(x, y)$, $f(x, y)$ and $\bar{f}(x, y)$ are edge mask, original image and blurred image respectively. We convert this process to CNN-based module. First, we generate an image from feature $F_{d,RECAB}$, which comes from RECAB, using one convolution layer:

$$I_{d,blockSR} = H_{d,blockSR}(F_{d,RECAB}), \quad (15)$$

where $I_{d,blockSR}$ is a produced image from feature $F_{d,eca}$, and $H_{d,blockSR}$ can be denoted as image reconstruction of d -th block in edge profile module, which generates RGB-channel image from the 64-channel feature. To form a blurred image, we transfer arithmetic mean filter concept using average pooling. Let's denote S_{xy} as the set of coordinates in a rectangular sub-image window of size $m \times n$ where center point is (x, y) . Then this filter computes the average values of the original image $i(x, y)$ in the area defined by S_{xy} . In other words,

$$\hat{i}(x, y) = \frac{1}{mn} \sum_{(s,t) \in S_{xy}} i(s, t), \quad (16)$$

where $\hat{i}(x, y)$ is a blurred image of $i(x, y)$. From this operation, if we define window size as 3×3 , it can also be average pooling operation. So we form the blurred image by using it.

$$I_{d,blockblur} = H_{d,blur}(I_{d,blockSR}), \quad (17)$$

where $I_{d,blockblur}$ is the blurred image from $I_{d,blockSR}$ and $H_{d,blur}$ denotes average pooling whose kernel size is 3×3 and padding margin is 1. From operation in Eq.14, to get a edge profile(or mask), $I_{d,blockSR}$ is subtracted by $I_{d,blockblur}$. Then we apply ReLU operation on edge profile(or mask) for getting outer line.

$$M_d = \text{ReLU}(I_{d,blockSR} \ominus I_{d,blockblur}), \quad (18)$$

where M_d denotes edge profile(or mask) in d -th block and \ominus is element-wise subtraction. To guide edge in training process, we concatenate $I_{d,blockSR}$ with M_d

$$I_{d,guided} = \text{Concat}(I_{d,blockSR}, M_d), \quad (19)$$

where $I_{d,guided}$ and $\text{Concat}(\cdot)$ denote a guided image and concatenation operation respectively. In the end, to generate

the feature of edge profile(EP) module, we apply one convolution layer, and then give the feature $F_{d,FE}$ information by using residual structure.

$$F_{d,EP} = F_{d,FE} + H_{d,EP}(I_{d,guided}), \quad (20)$$

where $F_{d,EP}$ stands for edge profile(EP) feature which channel size is 64 and $H_{d,EP}$ denotes edge profile module of d -th block.

Context network Module. To utilize information of edge profile feature effectively, we design a context network(CN) module based on dilated convolutions. By [48], context network is constructed to increase the performance of dense prediction structures by aggregating multi-scale contextual information. Furthermore, input and output features have the same form and number of feature maps. Thus the module can be plugged into existing dense prediction architectures.

Inspired by the concept, we apply a small context network module on each REEB. As CN part of Fig.2, our CN module consists of four 3×3 dilated convolution network, whose dilated factors are 1, 2, 4, and 1 in order. To prevent loss of resolution or coverage, we consider expansion of the receptive field to set up dilated factors exponentially. Intuitively, CN module can improve the accuracy of the feature maps by passing them through multiple layers that expose contextual information. After that, the output feature is added by the input feature as residual block.

$$F_{d,CN} = F_{d,EP} + H_{f=1} \circ H_{f=4} \circ H_{f=2} \circ H_{f=1}(F_{d,EP}), \quad (21)$$

where $F_{d,CN}$ is the output feature of CN module and $H_{f=n}(\cdot)$ denotes dilated convolution whose dilated factor f is n . As this operation captures contextual information from the feature of edge profile module $F_{d,EP}$, it plays a role as sharpening filter.

3.4. Implementation Details

We set fractal group number as $g = 7$ in the fractal skip connection module. So we utilize 128 blocks in network. In RECAB module, we set the size and number of filter as 3×3 and $C = 64$ in the feature extraction and use $k = 9$ which is 1D convolution filter size in ECA. Since the details of EP module are aforementioned, we skip it. All of the dilated convolutions in CN module also has $C = 64$ filters. we follow upscale module $H_{UP}(\cdot)$ which is proposed in [28, 55], and apply ESPCNN[37] to upscale the feature from FSC module. The reconstruction layer H_{Re} consists of one convolution operation, which has 3 filters to output color images.

4. Experiment Results

4.1. Settings

We state the settings of experiment about datasets, degradation models, evaluation, and training settings.

Datasets. Following [28, 54, 55], we set up 800 high resolution images from DIV2K dataset [43] as a training set. For testing, we use 5 standard benchmark datasets: Set5[3], Set14[49], B100[29], Urban100[18], and Manga109[30].

Degradation models. In order to prove the effectiveness of our EPSR, we use 3 degradation models to generate LR images. First, we generate LR images with scaling factor $\times 2$, $\times 3$, $\times 4$ by using Bicubic interpolation(BI) operation. Second, by using Gaussian kernel of size 7×7 with standard deviation 1.6, we blur HR image and downsample it with scaling factor $\times 3$. We denote this process as BD[52]. At last, we downsample HR image with scaling factor $\times 3$ using bicubic interpolation and then add Gaussian noise with level 30. This process is denoted as DN for short.

Evaluation metrics. The SR results are evaluated with PSNR and SSIM[45] on Y channel(i.e. luminance) of YCbCr space.

Training settings. In training process, the training images are augmented by randomly rotating $90^\circ, 180^\circ, 270^\circ$, and horizontally flipping. In each training batch, 8 LR color patches with size 48×48 are extracted as input. Our model is trained by ADAM optimizer with $\beta_1 = 0.9$, $\beta_2 = 0.99$, and $\epsilon = 1e - 8$. we set learning rate as 10^{-4} initially and then it is reduced to half every 200 epochs. We implement our proposed EPSR using Pytorch[32] on a Tesla V100 GPU.

4.2. Ablation study

As we discussed in section 3, our EPSR consists of 3 modules. we focus on the effect of edge profile(EP) module and context network(CN) module, and then we compared the difference between efficient channel attention and general channel attention based on channel reduction. we also clarify the reason why we apply not only L_1 loss but also $L_{gradient}$ loss.

Basicblock		Set5		Set14		BSD100		Urban100		Manga109	
		PSNR/SSIM		PSNR/SSIM		PSNR/SSIM		PSNR/SSIM		PSNR/SSIM	
RECAB	4	32.26/0.8937		28.46/0.7802		27.26/0.7327		26.29/0.7934		30.55/0.9017	
RECAB+EP	4	32.20/0.8932		28.51/0.7823		27.34/0.7356		26.31/0.7943		30.66/0.9062	
RECAB+CN	4	31.44/0.8786		22.75/0.5959		21.33/0.5206		19.40/0.5848		27.05/0.8274	
RCAB+EP+CN	4	32.25/0.8939		28.53/0.7831		27.32/0.7349		26.39/0.7975		30.73/0.9076	
RECAB+EP+CN	4	32.28/0.8945		28.55/0.7828		27.34/0.7362		26.43/0.7983		30.82/0.9084	

Table 1. Effects of different module. we report PSNR and SSIM values on all datasets($4 \times$).

Edge profile module and Context network module. To prove the effectiveness of edge profile(EP) module and context network(CN) module, we set four comparisons, which are based on fractal skip connection(FSC) structure. These comparisons are tested on all datasets and the specific performance is listed in Table 1.

First, we apply channel attention mechanism, which consists of residual efficient channel attention(RECAB) as a standard block for comparison on FSC structure. To verify the effectiveness of edge profile(EP) module, we plugged this module into the standard block. From Table.1, we can check that EP module brings about $0.03 \sim 0.11$ dB benefits in PSNR and $0.03 \sim 0.05$ benefits in SSIM. Although EP module gives just edge information to the features, this module improves the performance very well.

As we mentioned in Section 3, by adding CN module to EP module, we construct our REEB and can check that the contextual feature information from EP module are captured significantly. Thus these results verify the effectiveness of CN module and our EPSR together. However, when CN module is connected to RECAB module directly, we check that results reach overfitting. From these results, CN module could generate a significant synergy effect with EP module, and enhance significantly the result by exploiting contextual information in the features including edge information.

Efficient channel attention vs General channel attention.

To verify the efficiency of efficient channel attention(ECA) mechanism in our EPSR, we show the difference between efficient channel attention(ECA) and general channel attention(CA). As we discussed in Section 3, by substituting channel reduction to 1D convolution, the number of parameters is decreased. we set 1D convolution kernel size $k = 9$ in ECA and channel reduction $r = 16$ in CA. As shown in Table.1, although the module is 73k smaller than using CA, the former is better than the latter in the results.

Applying gradient loss. To prove the effectiveness of gradient loss, we optimize our model with L_1 loss and $L_{gradient}$ added to it respectively. With L_1 loss, our EPSR shows gradient exploding. However, with $L_1 + 0.1 \cdot L_{gradient}$, our model converges stably. Intuitively, $L_{gradient}$ would prevent to lose guiding edge information and also help to optimize it.

4.3. Results with BI

To compare the effectiveness of our network with other methods, we investigate 11 state-of-the-art CNN-based SR methods: SRCNN [8], FSRCNN [9], VDSR [22], LapSRN [26], EDSR [28], MemNet [41], IDN [19], SRMDNF [52], CARN [1], RDN [55], and RCAN [54]. Same as in [28, 54, 55], we apply self-ensemble method to further improve our EPSR, and we denote the process as EPSR+. All of the quantitative comparisons for $\times 2$, $\times 3$ and $\times 4$ SR are shown in Table.2. Compared with previous methods, EPSR+ shows competitive results with other state-of-the-art methods in all scaling factors. Without self-ensemble, EPSR also obtains very similar results which are in Top-3 methods.

With rich texture information datasets, such as Set5,

Set14, and BSD100, our EPSR obtains better results in SSIM compared to other networks. However, in PSNR, it obtains a little worse results. In Urban 100 and Manga109 datasets that contain rich repeated edge information, our EPSR achieves competitive results. Thus our EPSR works better on images with diverse information, such as texture and edge. These results show that utilizing image properties based on edge information is effective in CNN-based SR methods and edge profile prior concept is converted to CNN-based module successfully.

Table 2. Quantitative results with BI degradation model. **High-light** stands for the best performance, **red** indicates the second, and **blue** is the third.

Method		Set5		Set14		BSD100		Urban100		Manga109	
		PSNR/SSIM	PSNR/SSIM	PSNR/SSIM	PSNR/SSIM	PSNR/SSIM	PSNR/SSIM	PSNR/SSIM	PSNR/SSIM	PSNR/SSIM	PSNR/SSIM
Bicubic	2	33.66/0.9229	30.24/0.8688	29.56/0.8431	26.88/0.8403	30.80/0.9339					
SRCNN	2	36.66/0.9542	32.45/0.9067	31.36/0.8879	29.50/0.8946	35.60/0.9663					
FSRCNN	2	36.98/0.9556	32.62/0.9087	31.50/0.8904	29.85/0.9009	36.62/0.9710					
VDSR	2	37.53/0.9587	33.05/0.9127	31.90/0.8960	30.77/0.9141	37.16/0.9740					
LapSRN	2	37.52/0.9591	32.99/0.9124	31.80/0.8949	30.41/0.9101	37.53/0.9740					
EDSR	2	37.99/0.9587	33.57/0.9175	32.16/0.8994	31.98/0.9272	39.10/0.9773					
MemNet	2	37.78/0.9597	33.28/0.9142	32.08/0.8978	31.31/0.9195	37.72/0.9740					
IDN	2	37.83/0.9600	33.30/0.9148	32.08/0.8985	31.27/0.9196	38.02/0.9749					
SRMDNF	2	37.79/0.9601	33.32/0.9159	32.05/0.8985	31.33/0.9204	38.07/0.9761					
CARN	2	37.76/0.9590	33.52/0.9166	32.09/0.8978	31.92/0.9256	38.36/0.9764					
RDN	2	38.24/0.9614	34.01/0.9212	32.34/0.9017	32.89/0.9353	39.18/0.9780					
RCAN	2	38.27/0.9614	34.12/0.9216	32.41/0.9027	33.34/0.9384	39.44/0.9786					
EPSR	2	38.20/0.9614	34.04/0.9220	32.32/0.9039	33.12/0.9384	39.38/0.9782					
EPSR+	2	38.29/0.9618	34.13/0.9227	32.38/0.9046	33.36/0.9401	39.57/0.9788					
Bicubic	3	30.40/0.8686	27.54/0.7741	27.21/0.7389	24.46/0.7349	26.95/0.8556					
SRCNN	3	32.75/0.9090	29.29/0.8215	28.41/0.7863	26.24/0.7991	30.48/0.9117					
FSRCNN	3	33.16/0.9140	29.42/0.8242	28.52/0.7893	26.41/0.8064	31.10/0.9210					
VDSR	3	33.66/0.9213	29.78/0.8318	28.83/0.7976	27.14/0.8279	32.01/0.9340					
LapSRN	3	33.82/0.9227	29.79/0.8320	28.82/0.7973	27.07/0.8271	32.21/0.9350					
EDSR	3	34.37/0.9270	30.28/0.8418	29.09/0.8052	28.15/0.8527	34.17/0.9476					
MemNet	3	34.09/0.9248	30.00/0.8350	28.96/0.8001	27.56/0.8376	32.51/0.9369					
IDN	3	34.11/0.9253	29.99/0.8354	28.95/0.8013	27.42/0.8359	32.69/0.9378					
SRMDNF	3	34.12/0.9254	30.04/0.8382	28.97/0.8025	27.57/0.8398	33.00/0.9403					
CARN	3	34.29/0.9255	30.29/0.8407	29.06/0.8034	28.06/0.8493	33.49/0.9440					
RDN	3	34.71/0.9296	30.57/0.8468	29.26/0.8093	28.80/0.8653	34.13/0.9484					
RCAN	3	34.74/0.9299	30.65/0.8482	29.32/0.8111	29.09/0.8702	34.44/0.9499					
EPSR	3	34.60/0.9283	30.37/0.8465	29.06/0.8116	28.74/0.8661	34.13/0.9462					
EPSR+	3	34.73/0.9297	30.52/0.8491	29.15/0.8139	28.96/0.8702	34.46/0.9486					
Bicubic	4	28.43/0.8109	26.00/0.7023	25.96/0.6678	23.14/0.6574	25.15/0.7890					
SRCNN	4	30.48/0.8628	27.50/0.7513	26.90/0.7103	24.52/0.7226	27.66/0.8580					
FSRCNN	4	30.70/0.8657	27.59/0.7535	26.96/0.7128	24.60/0.7258	27.89/0.8590					
VDSR	4	31.35/0.8838	28.02/0.7678	27.29/0.7252	25.18/0.7525	28.82/0.8860					
LapSRN	4	31.54/0.8866	28.09/0.7694	27.32/0.7264	25.21/0.7553	29.09/0.8900					
EDSR	4	32.09/0.8938	28.58/0.7813	27.57/0.7357	26.04/0.7849	31.02/0.9148					
MemNet	4	31.74/0.8893	28.26/0.7723	27.40/0.7281	25.50/0.7630	29.42/0.8942					
IDN	4	31.82/0.8903	28.25/0.7730	27.41/0.7297	25.41/0.7632	29.40/0.8936					
SRMDNF	4	31.96/0.8925	28.35/0.7787	27.49/0.7337	25.68/0.7731	30.09/0.9024					
CARN	4	32.13/0.8937	28.60/0.7806	27.58/0.7349	26.07/0.7837	30.40/0.9082					
RDN	4	32.47/0.8990	28.81/0.7871	27.72/0.7419	26.61/0.8028	31.00/0.9151					
RCAN	4	32.63/0.9002	28.87/0.7889	27.77/0.7436	26.82/0.8087	31.22/0.9173					
EPSR	4	32.28/0.8945	28.55/0.7828	27.34/0.7362	26.43/0.7983	30.82/0.9084					
EPSR+	4	32.42/0.8969	28.65/0.7867	27.45/0.7403	26.64/0.8038	31.16/0.9127					

Visual quality. In Fig.4, we present visual comparison on scale $\times 4$. For image “img_076” and “img_093”, we observe that most of the compared models cannot reconstruct the lattices and would have trouble in blurring effects. Other methods, such as MemNet and SRMDNF, would generate twisted lines and squashed the lattices. However, our EPSR can alleviate the blurring artifact and make the details as edge and lattice more distinctly. In addition, our EPSR would generate lines and lattices in image with right direction. Compared with the ground-truth, our EPSR and RCAN reconstruct more faithful results and recover details clearly. These results verify the remarkable quality of EPSR with powerful representational ability. Although it is difficult to recover details and high frequency information

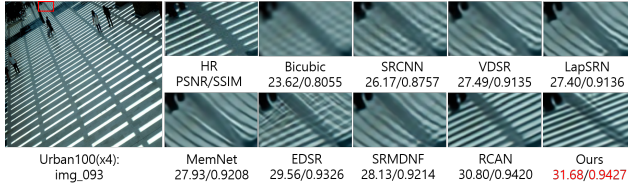


Figure 4. Visual Comparison for SR($\times 4$) with BI model on Urban100. The best results are **highlighted**

from LR images due to limited information, our EPSR can make effective use of diverse information through fractal skip connection structure, and simultaneously utilize channel feature correlations and edge profile information for more powerful representations. Therefore it can produce high quality results.

4.4. Results with BD and DN

We apply our EPSR with BD degradation model, which is used recently in [54], and following [55], we further compare various SR methods on image with DN degradation model. We compare our EPSR with 8-state-of-the-art SR methods with $\times 3$ scaling factors: SRMSR[33], SRCNN[8], FSRCNN[9], VDSR[22], IRCNN[51], SRMDNF[52], RDN[55], and RCAN[54]. In Table.3 and Table.4, all of the results are stated explicitly. we can observe that our EPSR shows competitive results in Top 3 even without self-ensemble. These results imply that our EPSR is very effective method for various types of degradation models. Specifically, edge profile and context network module function well in diverse degradation problems.

Table 3. Quantitative results with BD degradation model

Method		Set5	Set14	BSD100	Urban100	Manga109
		PSNR/SSIM	PSNR/SSIM	PSNR/SSIM	PSNR/SSIM	PSNR/SSIM
Bicubic	3	28.78/0.8308	26.38/0.7271	26.33/0.6918	26.88/0.8403	25.46/0.8149
SRMSR	3	32.21/0.9001	28.89/0.8105	28.13/0.7740	25.84/0.7856	29.64/0.9003
SRCNN	3	32.05/0.8944	28.80/0.8074	28.13/0.7736	25.70/0.7770	29.47/0.8924
FSRCNN	3	26.23/0.8124	24.44/0.7106	24.86/0.6832	22.04/0.6745	23.04/0.7927
VDSR	3	33.25/0.9150	29.46/0.8244	28.57/0.7893	26.61/0.8136	31.06/0.9234
IRCNN_G	3	33.38/0.9182	29.63/0.8281	28.65/0.7922	26.77/0.8154	31.15/0.9245
IRCNN_C	3	33.17/0.9157	29.55/0.8271	28.49/0.7886	26.47/0.8081	31.13/0.9236
SRMDNF	3	34.01/0.9242	30.11/0.8364	28.98/0.8009	27.50/0.8301	32.97/0.9391
RDN	3	34.58/0.9280	30.53/0.8447	29.23/0.8079	28.46/0.8582	33.97/0.9465
RCAN	3	34.70/0.9288	30.63/0.8462	29.32/0.8093	28.81/0.8645	34.38/0.9483
EPSR	3	34.54/0.9274	30.42/0.8458	29.05/0.8107	28.61/0.8627	34.18/0.9452
EPSR+	3	34.68/0.9288	30.56/0.8484	29.14/0.8130	28.83/0.8667	34.51/0.9476

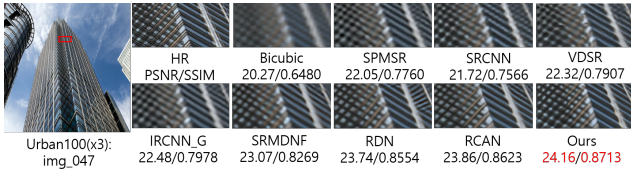


Figure 5. Visual Comparison for SR($\times 3$) with BD model on Urban100. The best results are **highlighted**.

Visual quality. We also show visual comparisons in Fig.5 and Fig.6. For challenging details in images “img_047” and “302008”, most methods suffer from heavy blurring and noising artifacts. EPSR alleviates these trouble significantly and can reconstruct more details compared to other



Table 4. Quantitative results with DN degradation model

Method		Set5	Set14	BSD100	Urban100	Manga109
		PSNR/SSIM	PSNR/SSIM	PSNR/SSIM	PSNR/SSIM	PSNR/SSIM
Bicubic	3	24.01/0.5369	22.87/0.4724	22.92/0.4449	21.63/0.4687	23.01/0.5381
SRCNN	3	25.01/0.6950	23.78/0.5898	23.76/0.5538	21.90/0.5737	23.75/0.7148
FSRCNN	3	24.18/0.6932	23.02/0.5856	23.41/0.5556	21.15/0.5682	22.39/0.7111
VDSR	3	25.20/0.7183	24.00/0.6112	24.00/0.5749	22.22/0.6096	24.20/0.7525
IRCNN_G	3	25.70/0.7379	24.45/0.6305	24.28/0.5900	22.90/0.6429	24.88/0.7765
IRCNN_C	3	27.48/0.7925	25.92/0.6932	25.55/0.6481	23.93/0.6950	26.07/0.8253
RDN	3	28.47/0.8151	26.60/0.7101	25.93/0.6573	24.92/0.7364	28.00/0.8591
EPSR	3	28.41/0.8068	26.46/0.7017	25.75/0.6482	25.01/0.7393	28.02/0.8567
EPSR+	3	28.53/0.8142	26.57/0.7105	25.86/0.6588	25.16/0.7477	28.20/0.8634



Figure 6. Visual Comparison for SR($\times 3$) with DN model on Urban100. The best results are **highlighted**.

methods such as IRCNN and RDN. In addition, EPSR can be comparable with RCAN. Although there is a heavy loss of information, our EPSR obtains very high performance by recovering more informative components and preventing distortions of information. These results indicate that edge profile with deep network would overcome various losses such as heavy noising and blurring problems. It also means the powerful ability of EPSR for BD and DN degradations.

5. Discussion and Future works.

In this paper, we propose our EPSR for single image SR by utilizing edge profile concept in a very deep neural network. Specifically, a fractal skip connection (FSC) structure allows our EPSR to bypass abundant information from low to high frequency components. Furthermore, to utilize the diverse information from this structure, we construct a residual edge enhance block(REEB). From residual efficient channel attention block(RECAB) module, adaptive rescale channel-wise features are extracted by considering channel inter-dependencies efficiently and then more informative features are generated by extracting edge profile itself from edge profile(EP) module. In the end, context network(CN) module improves details by learning contextual information of edge-guided features. Extension experiments on SR with BI, BD, and DN degradation models show the effectiveness of our EPSR.

As we convert edge profile concept to CNN-based module successfully, our method leads to an interesting direction in super-resolution by drawing a concept from image properties. This direction shows that just stacking deep network is not the only solution and image properties, such as edge information could help improving the super-resolution process.

References

- [1] Namhyuk Ahn, Byungkong Kang, and Kyung-Ah Sohn. Fast, accurate, and lightweight super-resolution with cascading residual network. In *Proceedings of the European Conference on Computer Vision (ECCV)*, pages 252–268, 2018. 7
- [2] Saeed Anwar and Nick Barnes. Densely residual laplacian super-resolution. *IEEE Transactions on Pattern Analysis and Machine Intelligence*, 2020. 3
- [3] Marco Bevilacqua, Aline Roumy, Christine Guillemot, and Marie Line Alberi-Morel. Low-complexity single-image super-resolution based on nonnegative neighbor embedding. 2012. 6
- [4] John Canny. A computational approach to edge detection. *IEEE Transactions on pattern analysis and machine intelligence*, (6):679–698, 1986. 2
- [5] Hong Chang, Dit-Yan Yeung, and Yimin Xiong. Super-resolution through neighbor embedding. In *Proceedings of the 2004 IEEE Computer Society Conference on Computer Vision and Pattern Recognition, 2004. CVPR 2004.*, volume 1, pages I–I. IEEE, 2004. 1
- [6] Jae-Seok Choi and Munchurl Kim. A deep convolutional neural network with selection units for super-resolution. In *Proceedings of the IEEE Conference on Computer Vision and Pattern Recognition Workshops*, pages 154–160, 2017. 3
- [7] Chao Dong, Chen Change Loy, Kaiming He, and Xiaoou Tang. Learning a deep convolutional network for image super-resolution. In *European conference on computer vision*, pages 184–199. Springer, 2014. 1
- [8] Chao Dong, Chen Change Loy, Kaiming He, and Xiaoou Tang. Image super-resolution using deep convolutional networks. *IEEE transactions on pattern analysis and machine intelligence*, 38(2):295–307, 2015. 1, 2, 4, 7, 8
- [9] Chao Dong, Chen Change Loy, and Xiaoou Tang. Accelerating the super-resolution convolutional neural network. In *European conference on computer vision*, pages 391–407. Springer, 2016. 3, 7, 8
- [10] Weisheng Dong, Lei Zhang, Guangming Shi, and Xiaolin Wu. Image deblurring and super-resolution by adaptive sparse domain selection and adaptive regularization. *IEEE Transactions on image processing*, 20(7):1838–1857, 2011. 1, 2
- [11] Mehran Ebrahimi and Edward R Vrscay. Solving the inverse problem of image zooming using “self-examples”. In *International Conference Image Analysis and Recognition*, pages 117–130. Springer, 2007. 1
- [12] Raanan Fattal. Image upsampling via imposed edge statistics. In *ACM SIGGRAPH 2007 papers*, pages 95–es. 2007. 1, 2, 3
- [13] William T Freeman, Thouis R Jones, and Egon C Pasztor. Example-based super-resolution. *IEEE Computer graphics and Applications*, 22(2):56–65, 2002. 1
- [14] William T Freeman, Egon C Pasztor, and Owen T Carmichael. Learning low-level vision. *International journal of computer vision*, 40(1):25–47, 2000. 1
- [15] Muhammad Haris, Gregory Shakhnarovich, and Norimichi Ukita. Deep back-projection networks for super-resolution. In *Proceedings of the IEEE conference on computer vision and pattern recognition*, pages 1664–1673, 2018. 2
- [16] Kaiming He, Xiangyu Zhang, Shaoqing Ren, and Jian Sun. Deep residual learning for image recognition. In *Proceedings of the IEEE conference on computer vision and pattern recognition*, pages 770–778, 2016. 1
- [17] Jie Hu, Li Shen, and Gang Sun. Squeeze-and-excitation networks. In *Proceedings of the IEEE conference on computer vision and pattern recognition*, pages 7132–7141, 2018. 4
- [18] Jia-Bin Huang, Abhishek Singh, and Narendra Ahuja. Single image super-resolution from transformed self-exemplars. In *Proceedings of the IEEE conference on computer vision and pattern recognition*, pages 5197–5206, 2015. 6
- [19] Zheng Hui, Xiumei Wang, and Xinbo Gao. Fast and accurate single image super-resolution via information distillation network. In *Proceedings of the IEEE conference on computer vision and pattern recognition*, pages 723–731, 2018. 7
- [20] Justin Johnson, Alexandre Alahi, and Li Fei-Fei. Perceptual losses for real-time style transfer and super-resolution. In *European conference on computer vision*, pages 694–711. Springer, 2016. 4
- [21] Tero Karras, Timo Aila, Samuli Laine, and Jaakko Lehtinen. Progressive growing of gans for improved quality, stability, and variation. *arXiv preprint arXiv:1710.10196*, 2017. 1
- [22] Jiwon Kim, Jung Kwon Lee, and Kyoung Mu Lee. Accurate image super-resolution using very deep convolutional networks. In *Proceedings of the IEEE conference on computer vision and pattern recognition*, pages 1646–1654, 2016. 1, 2, 4, 7, 8
- [23] Jiwon Kim, Jung Kwon Lee, and Kyoung Mu Lee. Deeply-recursive convolutional network for image super-resolution. In *Proceedings of the IEEE conference on computer vision and pattern recognition*, pages 1637–1645, 2016. 2
- [24] Jun-Hyuk Kim, Jun-Ho Choi, Manri Cheon, and Jong-Seok Lee. Ram: Residual attention module for single image super-resolution. *arXiv preprint arXiv:1811.12043*, 2018. 3
- [25] Junhyung Kwak and Donghee Son. Fractal residual network and solutions for real super-resolution. In *Proceedings of the IEEE Conference on Computer Vision and Pattern Recognition Workshops*, pages 0–0, 2019. 4
- [26] Wei-Sheng Lai, Jia-Bin Huang, Narendra Ahuja, and Ming-Hsuan Yang. Deep laplacian pyramid networks for fast and accurate super-resolution. In *Proceedings of the IEEE conference on computer vision and pattern recognition*, pages 624–632, 2017. 1, 2, 4, 7
- [27] Wei-Sheng Lai, Jia-Bin Huang, Narendra Ahuja, and Ming-Hsuan Yang. Fast and accurate image super-resolution with

- deep laplacian pyramid networks. *IEEE transactions on pattern analysis and machine intelligence*, 41(11):2599–2613, 2018. 4
- [28] Bee Lim, Sanghyun Son, Heewon Kim, Seungjun Nah, and Kyoung Mu Lee. Enhanced deep residual networks for single image super-resolution. In *Proceedings of the IEEE conference on computer vision and pattern recognition workshops*, pages 136–144, 2017. 1, 2, 3, 4, 5, 6, 7
- [29] David Martin, Charless Fowlkes, Doron Tal, and Jitendra Malik. A database of human segmented natural images and its application to evaluating segmentation algorithms and measuring ecological statistics. In *Proceedings Eighth IEEE International Conference on Computer Vision. ICCV 2001*, volume 2, pages 416–423. IEEE, 2001. 6
- [30] Yusuke Matsui, Kota Ito, Yuji Aramaki, Azuma Fujimoto, Toru Ogawa, Toshihiko Yamasaki, and Kiyoharu Aizawa. Sketch-based manga retrieval using manga109 dataset. *Multimedia Tools and Applications*, 76(20):21811–21838, 2017. 6
- [31] Jim R Parker. *Algorithms for image processing and computer vision*. John Wiley & Sons, 2010. 4
- [32] Adam Paszke, Sam Gross, Soumith Chintala, Gregory Chanan, Edward Yang, Zachary DeVito, Zeming Lin, Alban Desmaison, and A Antiga. and lerer. *Automatic differentiation in pytorch*, 2017. 6
- [33] Tomer Peleg and Michael Elad. A statistical prediction model based on sparse representations for single image super-resolution. *IEEE transactions on image processing*, 23(6):2569–2582, 2014. 8
- [34] Judith MS Prewitt. Object enhancement and extraction. *Picture processing and Psychopictorics*, 10(1):15–19, 1970. 2
- [35] Mehdi SM Sajjadi, Bernhard Scholkopf, and Michael Hirsch. Enhancenet: Single image super-resolution through automated texture synthesis. In *Proceedings of the IEEE International Conference on Computer Vision*, pages 4491–4500, 2017. 1, 4
- [36] Qi Shan, Zhaorong Li, Jiaya Jia, and Chi-Keung Tang. Fast image/video upsampling. *ACM Transactions on Graphics (TOG)*, 27(5):1–7, 2008. 1
- [37] Wenzhe Shi, Jose Caballero, Ferenc Huszár, Johannes Totz, Andrew P Aitken, Rob Bishop, Daniel Rueckert, and Zehan Wang. Real-time single image and video super-resolution using an efficient sub-pixel convolutional neural network. In *Proceedings of the IEEE conference on computer vision and pattern recognition*, pages 1874–1883, 2016. 3, 6
- [38] Wenzhe Shi, Jose Caballero, Christian Ledig, Xiahai Zhuang, Wenjia Bai, Kanwal Bhatia, Antonio M Simoes Monteiro de Marvao, Tim Dawes, Declan O’Regan, and Daniel Rueckert. Cardiac image super-resolution with global correspondence using multi-atlas patchmatch. In *International Conference on Medical Image Computing and Computer-Assisted Intervention*, pages 9–16. Springer, 2013. 1
- [39] Jian Sun, Zongben Xu, and Heung-Yeung Shum. Image super-resolution using gradient profile prior. In *2008 IEEE Conference on Computer Vision and Pattern Recognition*, pages 1–8. IEEE, 2008. 2, 3
- [40] Ying Tai, Jian Yang, and Xiaoming Liu. Image super-resolution via deep recursive residual network. In *Proceedings of the IEEE conference on computer vision and pattern recognition*, pages 3147–3155, 2017. 2, 4
- [41] Ying Tai, Jian Yang, Xiaoming Liu, and Chunyan Xu. Memnet: A persistent memory network for image restoration. In *Proceedings of the IEEE international conference on computer vision*, pages 4539–4547, 2017. 2, 4, 7
- [42] Mingxing Tan, Ruoming Pang, and Quoc V Le. Efficientdet: Scalable and efficient object detection. In *Proceedings of the IEEE/CVF Conference on Computer Vision and Pattern Recognition*, pages 10781–10790, 2020. 5
- [43] Radu Timofte, Eirikur Agustsson, Luc Van Gool, Ming-Hsuan Yang, and Lei Zhang. Ntire 2017 challenge on single image super-resolution: Methods and results. In *Proceedings of the IEEE conference on computer vision and pattern recognition workshops*, pages 114–125, 2017. 6
- [44] Qilong Wang, Banggu Wu, Pengfei Zhu, Peihua Li, Wangmeng Zuo, and Qinghua Hu. Eca-net: Efficient channel attention for deep convolutional neural networks. In *Proceedings of the IEEE/CVF Conference on Computer Vision and Pattern Recognition*, pages 11534–11542, 2020. 2, 4
- [45] Zhou Wang, Alan C Bovik, Hamid R Sheikh, and Eero P Simoncelli. Image quality assessment: from error visibility to structural similarity. *IEEE transactions on image processing*, 13(4):600–612, 2004. 6
- [46] Zhaowen Wang, Ding Liu, Jianchao Yang, Wei Han, and Thomas Huang. Deep networks for image super-resolution with sparse prior. In *Proceedings of the IEEE international conference on computer vision*, pages 370–378, 2015. 1
- [47] Chih-Yuan Yang, Chao Ma, and Ming-Hsuan Yang. Single-image super-resolution: A benchmark. In *European Conference on Computer Vision*, pages 372–386. Springer, 2014. 1, 2
- [48] Fisher Yu and Vladlen Koltun. Multi-scale context aggregation by dilated convolutions. *arXiv preprint arXiv:1511.07122*, 2015. 6
- [49] Roman Zeyde, Michael Elad, and Matan Protter. On single image scale-up using sparse-representations. In *International conference on curves and surfaces*, pages 711–730. Springer, 2010. 6
- [50] Kaibing Zhang, Xinbo Gao, Dacheng Tao, and Xuelong Li. Single image super-resolution with non-local means and steering kernel regression. *IEEE Transactions on Image Processing*, 21(11):4544–4556, 2012. 1
- [51] Kai Zhang, Wangmeng Zuo, Shuhang Gu, and Lei Zhang. Learning deep cnn denoiser prior for image restoration. In *Proceedings of the IEEE conference on computer vision and pattern recognition*, pages 3929–3938, 2017. 8
- [52] Kai Zhang, Wangmeng Zuo, and Lei Zhang. Learning a single convolutional super-resolution network for multiple degradations. In *Proceedings of the IEEE Conference on Computer Vision and Pattern Recognition*, pages 3262–3271, 2018. 6, 7, 8
- [53] Lei Zhang and Xiaolin Wu. An edge-guided image interpolation algorithm via directional filtering and data fusion. *IEEE transactions on Image Processing*, 15(8):2226–2238, 2006. 1, 2

- [54] Yulun Zhang, Kunpeng Li, Kai Li, Lichen Wang, Bineng Zhong, and Yun Fu. Image super-resolution using very deep residual channel attention networks. In *Proceedings of the European Conference on Computer Vision (ECCV)*, pages 286–301, 2018. [1](#), [2](#), [4](#), [5](#), [6](#), [7](#), [8](#)
- [55] Yulun Zhang, Yapeng Tian, Yu Kong, Bineng Zhong, and Yun Fu. Residual dense network for image super-resolution. In *Proceedings of the IEEE conference on computer vision and pattern recognition*, pages 2472–2481, 2018. [1](#), [2](#), [3](#), [4](#), [6](#), [7](#), [8](#)
- [56] Wilman WW Zou and Pong C Yuen. Very low resolution face recognition problem. *IEEE Transactions on image processing*, 21(1):327–340, 2011. [1](#)